

APPLICATION OF PROBABILISTIC METHODS TO WEAPON RELIABILITY ASSESSMENT

Ben H. Thacker*, David S. Riha†
 Southwest Research Institute
 San Antonio, TX 78238

Edward A. Rodriguez‡, Jason E. Pepin‡
 Los Alamos National Laboratory
 Los Alamos, NM 87545

Abstract

Southwest Research Institute in collaboration with engineers at Los Alamos National Laboratory (LANL) are currently developing capabilities to provide reliability-based structural evaluation techniques for performing weapon component and system reliability assessments in support of eventual weapon certification by analysis. Focus herein is placed on two problems recently studied: 1) The uncertain structural response of an explosive actuated valve-piston assembly, and 2) the quasi-static collapse response of a spherical shell. The probabilistic dynamic response of the piston is evaluated through the coupling of the probabilistic software NESSUS (Numerical Evaluation of Stochastic Structures Under Stress)² with the non-linear structural dynamics code, ABAQUS/Explicit³. The probabilistic model includes variations in piston mass and geometry, and mechanical properties, such as Young's Modulus, yield strength, and flow characteristics. The probabilistic response of the shell is evaluated through the coupling of the NESSUS software and the explicit dynamic code DYNA3D⁵. Variations in geometric shape parameters and material properties are considered.

Nomenclature

%e	Percent elongation
%RA	Percent reduction of area
CDF	Cumulative density function
COV	Coefficient of Variation (μ/σ)
CVN	Charpy V-Notch (ft-lb)
e	elongation
E	Young's Modulus, (psi)
F_{tu}	tensile ultimate strength
F_{ty}	tensile yield strength
g	performance function
H()	higher order terms
n	strain hardening exponent
nrV	number of random variables
pdf	Probability density function
P_{RP}	Reaction product gas pressure, (psi)
RA	reduction in area
R_b	Rockwell hardness level b

R_c	Rockwell hardness level c
S_u	engineering ultimate strength
S_y	engineering yield strength
u	normal random variable
VISAR	Velocity interferometer
V_O	Impact velocity, (in/s)
X	random variable
x	value of random variable
Z	response variable

Greek Symbols

α	probabilistic sensitivity factor
β	safety index
γ_{UT}	True failure strain, (in/in)
:	Mean
<	Poisson's ratio
σ	Standard deviation
σ_{Ut}	True ultimate tensile strength, (ksi)

Introduction

Current arms control agreements have provided the impetus for national directives to cease production of new strategic weapons and end nuclear testing. This has placed a tremendous burden on the national laboratories for assuring stockpile certification. The Stockpile Stewardship Program's fundamental objective within the Department of Energy (DOE) is to maintain a high confidence in the safety, reliability, and performance of the existing U.S. nuclear weapons stockpile.

Enhanced evaluation capabilities are needed to determine the effect of possible anomalies that may arise in a weapon, e.g., due to aging mechanisms, and assess its performance, safety, and reliability. Experimental data and validated numerical models must be employed in determining the reliability of weapon components, including the weapon system. The validated numerical models must be based on accurate information the component's geometry and material properties, e.g., in an aged condition. Once these variables are known, extrapolation of potential lifetime of the weapon can be determined with some level of confidence. The goal at

* Principal Engineer, Senior Member AIAA

† Senior Research Engineer, Member AIAA

‡ Technical Staff Member

Copyright © 2001 Southwest Research Institute.

Published by the American Institute of Aeronautics and Astronautics, Inc. with permission.

Los Alamos is to develop an engineering capability that provides a reliability-based structural evaluation technique for performing weapon reliability assessments.

This paper describes recent work to compute the probabilistic structural response of an explosive actuated valve-piston and the collapse stability of a stainless-steel spherical shell. The valve and piston assembly was chosen because of its geometric simplicity, leading to an axisymmetric idealization, and because numerous laboratory-bench test have been conducted resulting in a statistically significant distribution. The stainless-steel shell model, which is actually a commercially available spherical marine float, was chosen because of its simple shape, yet highly complex nonlinear deformation behavior, leading to complex states-of-stress. There is also variability associated with the geometry and mechanical properties of the shell, which is not uncommon and principally due to numerous forming processes, different operators, etc.

The probabilistic analysis is performed using the NESSUS probabilistic analysis software, developed by Southwest Research Institute². NESSUS simulates uncertainties in loads, geometry, material behavior, and other user-defined uncertainty inputs to compute reliability and probabilistic sensitivity measures. To facilitate analyses of a broad range of problem types, a large number of efficient and accurate probabilistic methods are included in NESSUS.

Description Of Valve-Piston Assembly

The valve actuator uses a small amount of lead-styphnate explosive powder to propel a 0.5-inch (nominal) diameter piston down the valve barrel. An electrical signal is passed through a bridge-wire in the actuator, which in turn heats the lead-styphnate explosive initiating a burn. The pressure build-up from the deflagration, within the actuator void space, exceeds the strength of a thin stainless steel diaphragm, and subsequently allows the pressurized gas to expand and propel the piston down the valve barrel.

Two 0.125-inch (nominal) diameter stainless steel tubes protrude about 0.125-inch from the valve body. The tubes are severed by the piston cutter ring during travel. The severed tubes provide a means for pressurized gas transfer from the supply reservoir to the receiver reservoir. The piston cutter ring impacts upon a small “ledge” on the valve body at the end-of-travel, which is designed to mitigate the piston impact energy. In test firings, pistons have been observed to “over travel.” Piston over travel occurs when the cutter ring shears-off as it impacts the valve body ledge, then continues towards the sealed end of the valve body. Figure 1 shows a normal travel piston and an over travel piston.

The reaction products pressure boundary is maintained by a thin copper obturator, situated immediately above a Buna-N o-ring seal. The obturator is slightly larger in diameter than the piston outer diameter, and is held in-place by a set-screw. The interference fit between the obturator and valve barrel ensures a proper seal. The effect of o-ring friction is not taken into consideration. This assumption is reasonable because actual VISAR measurements of previous piston firings have

recorded the impact velocity at the valve ledge. This treatment assumes energy dissipation mechanisms are inherently included with the initial impact velocity. An axisymmetric representation is shown in Figure 2 below.

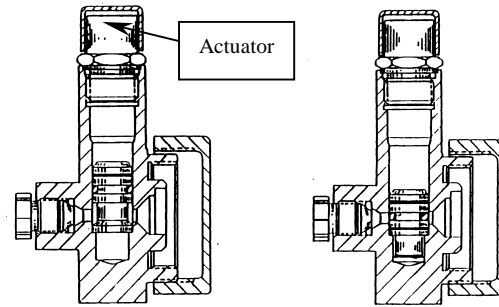


Figure 1. Piston (a) at valve stop and, (b) over travel.

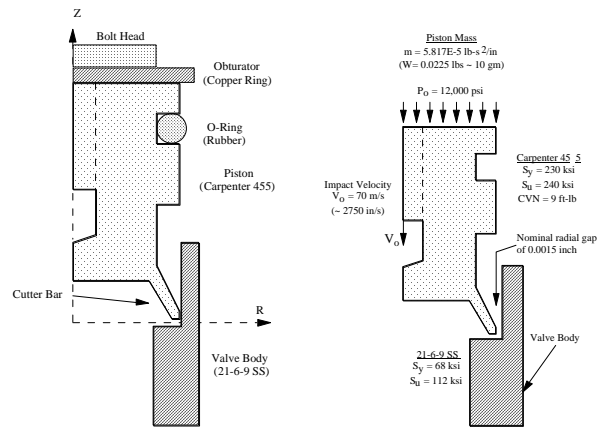


Figure 2. Axisymmetric representation of valve/piston.

Material Properties

Material characterization performed on both the valve body material 21-6-9 and Carpenter 455 stainless steel fall within the minimum specified properties. Table 1 presents mechanical properties for the nominal case, where σ_{Ut} and ϵ_{Ut} are the true ultimate tensile strength and strain to failure, and n is the strain-hardening exponent.

Table 1. Nominal Material Properties

Material	S_Y (ksi)	S_U (ksi)	%e	σ_{Ut} (ksi)	ϵ_{Ut} (in/in)	n
455	235	245	8	290	0.60	0.05
21-6-9	68	112	48	180	1.2	0.18

Interestingly, Carpenter 455 material exhibits a linearly decreasing fracture toughness characteristic as a function of aging temperature. Carpenter 455 appears to have a nominal fracture toughness of around 40 ksi(in)^{1/2}. Specifications show a tolerance of +/-10 °F from the target aging temperature. This would correspond to a nominal fracture toughness at 890°F of 35 ksi(in)^{1/2}. Although not considered

herein as a random variable, the material toughness may play an important role.

The valve body is a forging manufactured from a low carbon, austenitic, 21-6-9 stainless steel (i.e., 21%Cr, 6%Ni, 9%Mn). This steel is strain-rate sensitive with significant yield strength increase at successively higher strain rates. The ultimate strength of the material does not increase as significantly as the yield strength, but nevertheless does attain a slight increase.

For piston velocities within the range of 70 m/s impact on the 21-6-9 material, it is not uncommon to developed strain-rates within the range of $1E+3$ to $1E+4$ (sec^{-1}). Thus, it's expected that the actual yield strength of this material would be around 2 to 3 times the nominal static or quasi-static yield strength.

The stainless steels tubes, which are severed by the piston, will not be addressed. Because piston impact velocities are imposed, all other energy dissipation mechanisms prior to impact are ignored. As with the piston o-ring, no numerical analysis particular to the tubes is performed. Thus, the energy dissipation mechanisms are inherently taken into consideration within the initial impact velocity.

Design Criteria

Structural failure of the piston constitutes a 360° fracture of the cutter ring (i.e., skirt) upon impact with the valve body ledge. Three possible failure conditions exist;

1. Ductile failure: due to the magnitude of net-section plastic strains at the failure strain of the material,
2. Brittle fracture: applied stress intensity factor at the crack tip and the material's fracture toughness.
3. Bi-modal failure: ductile-to-brittle transition caused from void growth progressing to fracture.

Ductile Failure. Kinetic energy in the piston and reaction products back-pressure act simultaneously upon impact with the valve body to produce a region of high plastic strain. When a localized region is subjected to high plastic strains, micro-voids are created in the material. Continual plastic straining of adjacent locations may ensue, thus creating further voiding of material. Coalescence of these voids creates a localized ductile failure of the region. Progressive high plastic straining and void coalescence increases and ultimately through the thickness of the cutter ring, until complete ductile failure occurs.

Ductile failure criteria is governed by the von Mises yield criterion, where for axisymmetric model representations, the von Mises yield criterion reduces to:

$$\sigma_1^2 - \sigma_1\sigma_2 + \sigma_2^2 = Y^2 \tag{1}$$

where, σ_1, σ_2 = Principal stresses

Y= Yield strength

For ductile failure to occur, the assumption is that the material response is near the upper-shelf of the fracture toughness

curve. In this regime, ductile void nucleation, void growth, and void coalescence is assumed to occur. Herein, however, plastic shear strains are observed as indicators of potential piston fracture.

For true failure, a complete net-section plastic shear strain exceeding a tensile value of 30% is expected. As will be seen in the results, localized strain conditions exist that are near this limit, but do not extend through net section. The other two failure modes, brittle fracture and bi-modal, are not evaluated herein, yet are proposed for future investigation. Although the fracture mode is not evaluated, resulting plastic shear strains developed upon impact may transition from void growth to ductile fracture.

Deterministic Analysis Model

The numerical model forcing functions are the dynamic (i.e., inertial) impact velocity and the back-pressure on the piston, resulting from the reaction products deflagration. Material properties and inertial loads are initially treated deterministically to assess the state-of-strain for the "nominal" condition. The dynamic analysis model, as depicted in Figure 3, is an idealized axisymmetric representation of the valve/piston. Energy absorption in the valve body, from piston impact, is assumed localized in the lower portion of the valve. Therefore, only a portion of the valve body is modeled, specifically a region where the piston impacts on the valve ledge. A 0.0015" diametral gap is maintained initially as the piston impacts the valve body.

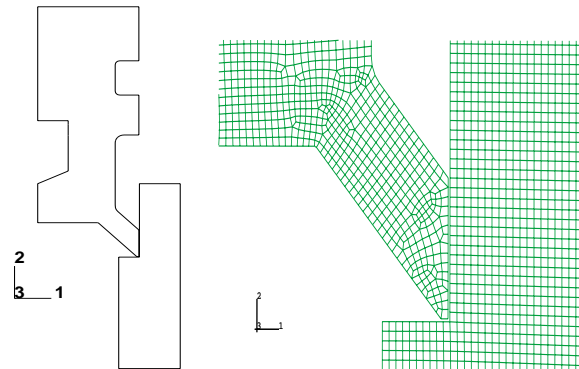


Figure 3. Piston and valve, axisymmetric model.

Initial piston impact velocity was calculated in the range of 70 m/s, which was confirmed from VISAR data in earlier tests conducted in the 1980's. Furthermore, detailed physics modeling and analyses using an Interior Ballistics Code has provided better approximation of the range of possible impact velocities based on the chemical kinetics of lead-styphnate deflagration. Current information suggests a distribution of impact velocity with the median at 70 m/s. Thus, potentially large variations in initial impact velocity are attained, ranging from 50 - 90 m/s.

Although energy losses arising from obturator/valve-barrel friction and tube-cutting are not taken into consideration, an accurate representation of initial impact velocity is adequate for the solution, hence no additional energy losses need be

accounted. This also serves in making the transient problem tractable from the standpoint of numerical analysis time integration.

Figure 4 depicts the piston cutter ring penetration into the valve body ledge approximately 0.015-inch, at the end of the transient. While nominal loading parameters and material properties are used in this deterministic analysis, the amount of piston penetration into the valve ledge is within 5-10% of that observed in a damaged valve body. This provides a clear indication that the loading and material parameters, especially the strain rate sensitive material, are within reasonable bounds.

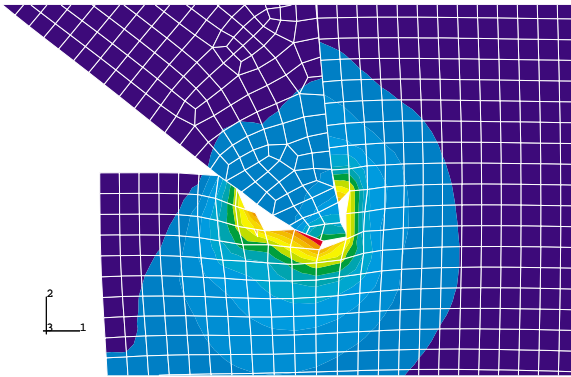


Figure 4. Piston penetration into valve body.

Figure 5 shows the temporal equivalent plastic stress at maximum impact response. The region of concern is a vertical plane, passing through the net section of the cutter ring thickness, which depicts stresses in excess of 260 ksi extending over 1/3 of the ring thickness.

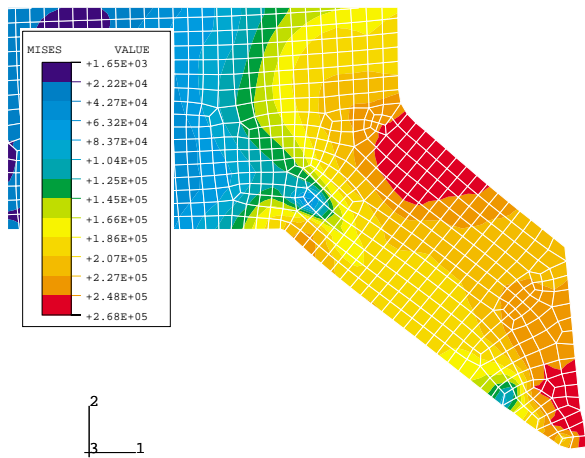


Figure 5. Equivalent plastic stress in piston cutter ring.

Sensitivity Analysis

A deterministic sensitivity analysis was initiated to study a few of the random variables surmised to have significance in the overall structural response. The deterministic model was

exercised by varying specific parameters. This was initially accomplished as a basis for further probabilistic structural analyses, which would take into consideration many more random variables. In these set of analyses, the following variables were varied, resulting in a total of twelve (12) separate finite element runs:

1. Impact velocity; ($V_1 = 70$ m/s and $V_2 = 90$ m/s)
2. Piston mass; (Nominal, Maximum, Minimum)
3. Cutter ring thickness; (Nominal, and Minimum)

Figure 6 provides the resultant plastic shear strains for the nominal piston cutter ring thickness case, for two separate impact velocities. It's quite evident that for the high impact velocity case, failure is inevitable. The nominal velocity case shows moderately high plastic shear strains, which may exceed the failure shear strain for a given set of conditions, yet does not extend through the net section.

Figure 7 shows the plastic shear strain as a function of thickness for three impact velocities. Important to note herein is that the velocity variation is approximately $\pm 2\sigma$ (standard deviations), and the thickness variation is nominal to -3σ . As such, for $+3\sigma$ level on piston cutter thickness, there would be little to no failures expected, based on the deterministic sensitivity analysis.

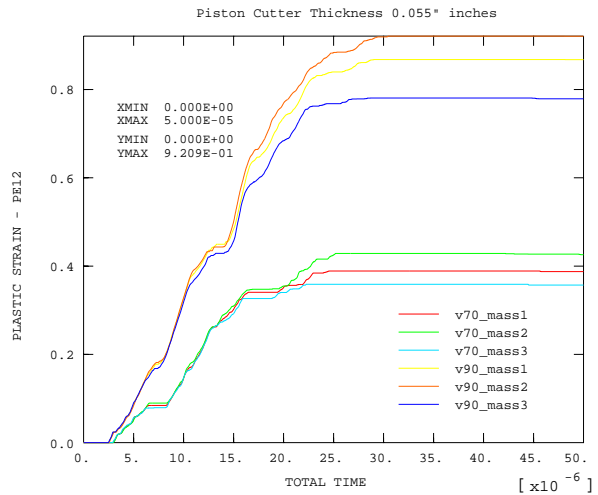


Figure 6. Plastic shear strains for nominal cutter ring thickness.

Description Of Marine Float

The structural components are “off-the-shelf,” commercially available, marine floats commonly used by the petro-chemical industries in large open, or closed, tanks for liquid level (gage) measurements. The marine floats were purchased directly from Quality Float Works in Shaumburg, IL, with a 9-inch outside diameter, 16-gage shell thickness, and no optional external piping connection. The goal was to obtain spherical shapes with as little as possible of any external structural perturbations, such as connections, thus limiting the complexity in collapse behavior. Nevertheless, each float has a small closure connection at the north pole that is used a final

seal. For the experimental collapse process, the north pole seal is drilled to release entrapped air during compression.

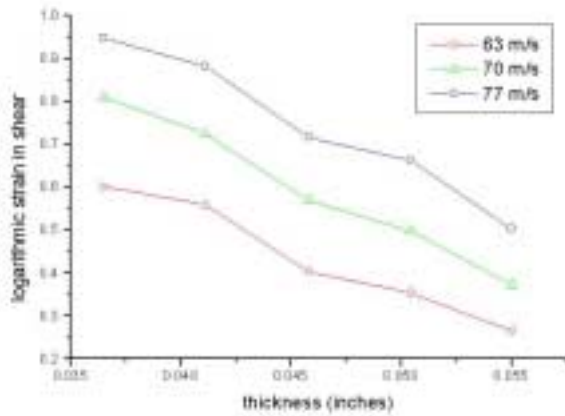


Figure 7. Plastic shear strains vs. cutter ring thickness.

No information was available from the manufacturer relative to whether the 100 floats purchased were from a single, or different, material lot. Also, because many liquids used in the petro-chemical industry are corrosive to metals, the choice material for marine floats is stainless steel, Type 316 or 304L. This is also fortuitous since 304L stainless steel is a well known and characterized material in the commercial nuclear industry. This implies that statistical variations in mechanical properties are readily available and may be used to compare with actual float characterization. However, actual material testing of a specified set of floats would provide better information on the variations within a single float, among several floats, and possibly within a material lot.

Small compression coupons, taken from a single marine float, were tested to determine their mechanical properties and also obtain a measure of their variation. Figure 8 shows the number of coupons, and the region, where the samples were taken. Although, the figure shows numerous samples taken from one region, the samples were actually taken from the complete periphery (i.e., 360°). This allows a better approximation of the variation in properties throughout the float. Table 2 shows the results of the compression tests compared to “as-received” 304L in plate stock.

Figure 9 shows the typical true stress-true strain curves for the different sections of the marine float. It is evident from Table 2 that extensive cold-work has been applied to the hemispherical shells, especially within the equatorial region. Figure 10 provides a measure of mechanical properties as a function of cold-work, suggesting that the equatorial region has received approximately 50% cold-work. This has been confirmed in discussions with the manufacturer, such that the drawing (or hydraulic pressing) process applies slightly higher cold-work on the flat sheet stock around the equatorial region.

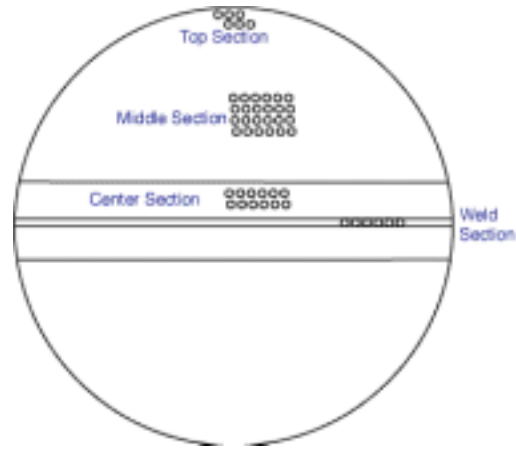


Figure 8. Compression coupons locations.

Table 2. Mechanical Properties.

	S_y (ksi)	S_u (ksi)	n
304L As-Received	32.0	75.0	0.25
Weld	51.0	88.5	0.28
Center (Equatorial)	123.0	170	0.10
Middle	77.0	117	0.22
Top	68.5	118	0.23

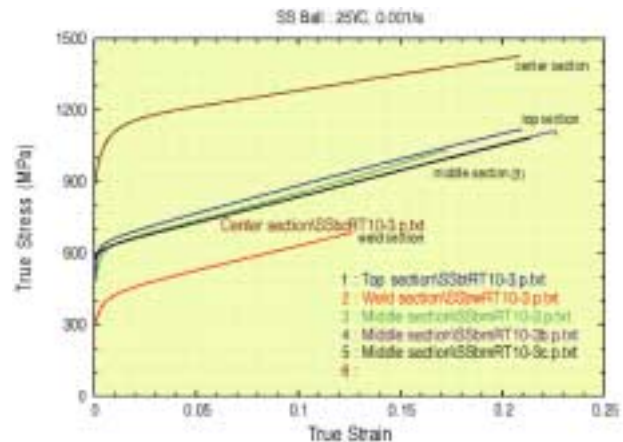


Figure 9. Stress strain data.

As previously stated, the floats are drawn into hemispherical shells from flat circular plate stock using a hydraulic press. The flat plate stock would have the nominal mechanical properties for common 304L plate/sheet. Once the hemispherical shells are pressed, each hemisphere is placed upon an automatic turning fixture for welding. Gas tungsten arc welding (GTAW), or commonly termed “tungsten inert gas” (TIG), is employed with helium as the shield gas to maintain an uncontaminated weld. The hemispheres are then welded at the equator, from the outside only, applying a 1/8-inch bead in a continuous process.

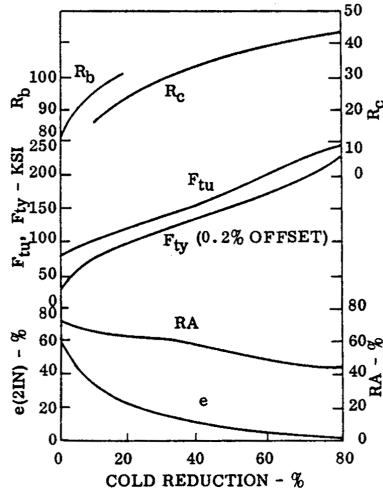


Figure 10. Effect of cold-work on 304L¹.

Deterministic Analysis

Model. The simulation of a marine float being crushed between two platen strokes was performed using DYNA3D, a nonlinear, explicit, Lagrangian finite element analysis code for three-dimensional transient structural mechanics⁵. The float was meshed with 15,600 quadrilateral shell elements into three distinct regions, the weld, a center band, and poles. The three regions are necessary in order to use different constitutive models to accurately model the mechanical behavior of the steel. A tabular elastic-plastic material model was used to model each region. The measured true stress, true strain curves as well as the elastic-plastic models are shown in Figure 12. A single hexahedral element was used to mesh each of the platens. The platens are modeled as rigid body material. The bottom platen is held fixed and the top platen is given a constant velocity to crush the float.

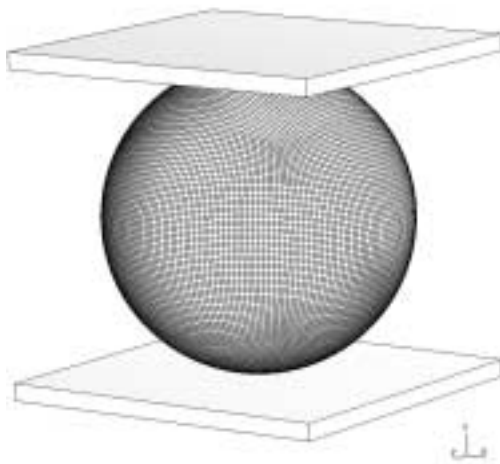


Figure 11. The mesh used for the marine float and platens.

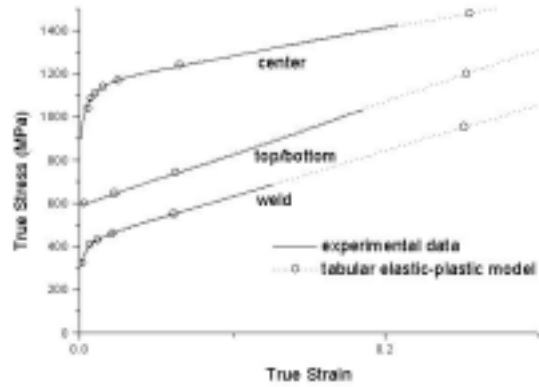


Figure 12. Stress-strain curves used to represent the SS304L material behavior.

Results. As an explicit finite element code, DYNA3D uses a large number of extremely small time steps to solve the governing equations for any given problem. This makes DYNA3D an efficient and ideal code for simulating transient events that occur in fractions of a second. The float, however, is crushed at 2 in/s. When simulating this quasi-static event, a compromise must be made between crush velocity and computational efficiency. Figure 13 shows the force required to crush the float for three different velocities. When the top platen is moving down at 10 m/s, a significant amount of dynamic noise can be seen in the force curve for the first 4.5 inches followed by a sharp spike up to 75,000 pounds at 5.5 inches. At 5 and 1 m/s, the dynamic noise has disappeared and the analysis is converging on a solution. Although the 1 m/s analysis may be a better quasi-static solution, it takes approximately 8 days, or 192 hours, of cpu time on a single processor to run. The 5 m/s analysis provides the best compromise between computational efficiency and a quasi-static solution. The solution is similar to the 1 m/s case and uses only 2 days of cpu time. Because a probabilistic analysis requires several simulations to be run as random variables are perturbed, it was decided to use the 5 m/s case as the nominal, or mean value, analysis.

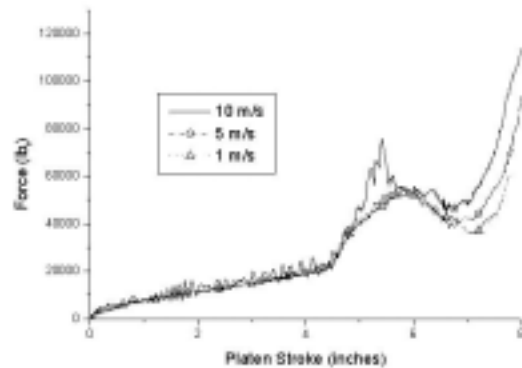


Figure 13. Force required to crush the float at three different velocities.

To date, twelve floats have been crushed experimentally. The load deflection curves for these floats are plotted with the nominal, 5 m/s, analysis in Figure 14. The hydraulic press used to crush the floats has a maximum stroke of four inches. As such, the floats must be crushed in two steps resulting in the unloading and then reloading seen between 3.5 and 4 inches. The force required to crush the floats is slightly higher than calculated for the first 4.5 inches. Since the two hemispheres for each float are pressed from flat plates, there is an increase in work hardening from the pole down to the equator. It is reasonable to assume that there is a gradual increase in material strength from the pole to the equator. The analysis assumes a discontinuous jump in material strength based on the limited testing of one float as described above. At 4.5 inches, the platens have crushed the finite element model to the higher strength center band. From this point on, the calculated force closely matches the force curves found from experiment.

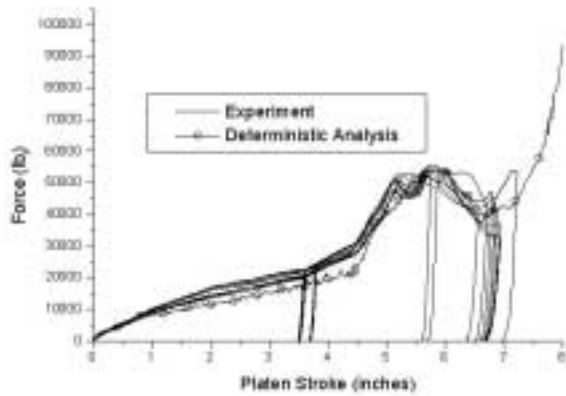


Figure 14. Comparison of experimental and deterministic force v. stroke curve.

A comparison between one of the crushed floats and the analysis can be made in Figure 15. During the experiment, the floats were consistently crushed into five lobes. The analysis displays similar buckling characteristics except that only four lobes develop. Unlike the actual floats, the finite element model is based on the geometry of a perfect sphere. Slight inconsistencies in geometry and material properties that can easily arise from the manufacturing process are not incorporated in the model. It is believed that these small differences result in the sphere being crushed into five lobes as opposed to four. It is clear from a cursory look at the deterministic analysis that the complicated structural response of the floats is not entirely incorporated in the model. However, the deterministic model reproduces the response of interest with sufficient accuracy to proceed on with the probabilistic analysis.

Probabilistic Analysis Methods

Efficient probabilistic methods were used to calculate the probabilistic response. These methods have been primarily developed for complex computational systems requiring time-consuming calculations, the results of which have been shown to approach the exact solution obtained from traditional

Monte Carlo methods using significantly fewer function evaluations⁴.

The limit-state (or g -) function can be defined as

$$g = Z(\mathbf{X}) - z_0 \quad (2)$$

where z_0 is a particular value of the response function, $Z(\mathbf{X})$ and \mathbf{X} is the vector of nrv random variables. The condition $g = 0$ defines the limit-state surface, which separates the variable space into failure ($g \leq 0$) and non-failure ($g > 0$) regions. Probability of failure, p_f , can then be defined as

$$p_f = \Pr[Z(\mathbf{X}) \leq z_0] = \Pr[g \leq 0] \\ = \int_{\Omega} \dots \int_{f_x(\mathbf{X})} d\mathbf{X} \quad (3)$$

where $f_x(\mathbf{X})$ is the joint p.d.f. of \mathbf{X} and Ω is the failure region defined where $g \leq 0$. It is important to understand that the phrase “probability of failure” means only that the limit-state criterion is violated. Thus, if the limit-state is defined in terms of a failure metric, e.g., fracture or buckling, then “probability of failure” could imply an actual failure mechanism, or that the structure is unfit to serve its intended purpose. On the other hand, if the limit-state is defined in terms of a model response, then “probability of failure” means only that the response has been exceeded, which may or may not relate to “failure” directly.

The p_f corresponding to $z_0 = 0$ defines one point in the cumulative distribution function (cdf.); the complete cdf. can be constructed by repeating the calculation of p_f for several different z_0 values. The joint pdf. in terms of iso-probability contours, limit-state, and failure region is illustrated in Figure 16 for the case of two random variables.

Except for a few trivial cases, Equation 2 requires numerical solution such as Monte Carlo simulation. However, if Equation 1 involves a complicated finite element model and/or if p_f is relatively small, Monte Carlo simulation can become impractical due to the large number of simulations needed to reduce sampling error to an acceptable level. Therefore, it is often desirable to use approximate methods, such as most probable point methods, that are more efficient than Monte Carlo simulation. Several such methods are implemented in the NESSUS computer program² and are suitable for this application. NESSUS has a built-in finite element structural modeling capability and interfaces to many other commercial finite element programs, and can simulate uncertainties in the loads, geometries, material behavior, and other user-defined uncertainty inputs.

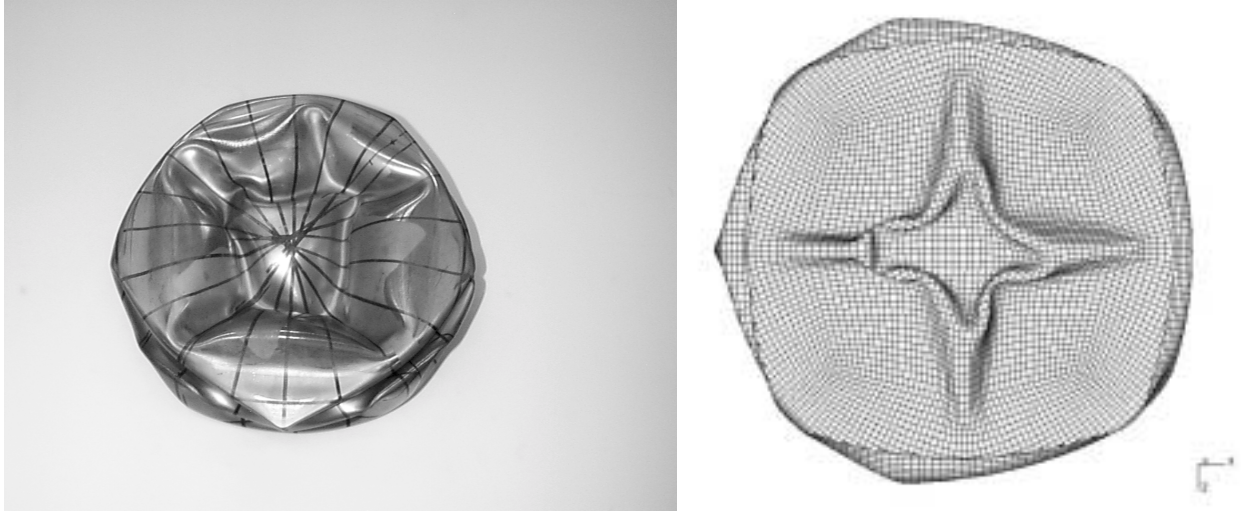


Figure 15. Comparison of experiment with deterministic analysis at a platen stroke of 7 inches.

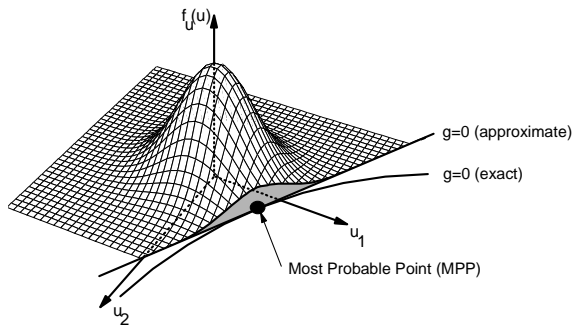


Figure 16. Joint probabilistic density function in standard normal space showing exact and approximate g -function and most probable point.

Most Probable Point (MPP) Methods

A class of probabilistic methods based on the most probable point (MPP) are becoming routinely used as a means of reducing the number of g -function evaluations from that of brute-force Monte Carlo simulation. Although many variations have been proposed, the best-known and most widely-used MPP-based methods include the first-order reliability method (FORM), second-order reliability method (SORM), and advanced mean value (AMV).

The basic steps involved in MPP-based methods are as follows: (1) Obtain an approximate fit to the exact g -function at X^* , where X^* is initially the mean random variable values; (2) Transform the original, non-normal random variables into independent, normal random variables u ; (3) Calculate the minimum distance, β (or safety index), from the origin of the joint p.d.f. to the limit state surface, $g = 0$. This point, u^* , on the limit state surface is the most probable point (MPP) in the u -space; (4) Approximate the g -function $g(u)$ at u^* using a

first or second-order polynomial function; and (5) Solve the resulting problem using available analytical solutions.

Step (1), which involves evaluating the g -function, represents the main computational burden in the above steps. Once a polynomial expression for the g -function is established, it is a numerically simple task to compute the failure probability and associated MPP. Because of this, the complete response cdf. can be computed very quickly by repeating steps (2)-(4) for different z_0 values. The resulting locus of MPP's is efficiently used in the advanced mean value algorithm (discussed next) to iteratively improve the probability estimates in the tail regions.

Advanced Mean Value (AMV) Method

The advanced mean value class of methods are most suitable for complicated but well-behaved response functions requiring computationally-intensive calculations⁷. Assuming that the response function is smooth and a Taylor's series expansion of Z exists at the mean values, the mean value Z -function can be expressed as

$$Z_{MV} = Z(\mu) + \sum_{i=1}^n \frac{\partial Z}{\partial X_i} \Big|_{\mu} (X_i - \mu_i) + H(X) \quad (4)$$

where Z_{MV} is a random variable representing the sum of the first order terms and $H(X)$ represents the higher-order terms.

For nonlinear response functions, the MV first-order solution obtained by using Equation 1 may not be sufficiently accurate. For simple problems, it is possible to use higher-order expansions to improve the accuracy. For example, a mean-value second-order solution can be obtained by retaining second-order terms in the series expansion. However, for problems involving implicit functions and large n , the higher-order approach becomes difficult and inefficient.

The AMV method improves upon the MV method by using a simple correction procedure to compensate for the errors introduced from the truncation of the Taylor's series. The AMV model is defined as

$$Z_{AMV} = Z_{MV} + H(Z_{MV}) \quad (5)$$

where $H(Z_{MV})$ is defined as the difference between the values of Z_{MV} and Z calculated at the Most Probable Point Locus (MPPL) of Z_{MV} , which is defined by connecting the MPP's for different z_0 values. The AMV method reduces the truncation error by replacing the higher-order terms $H(X)$ by a simplified function $H(Z_{MV})$. As a result of this approximation, the truncation error is not optimum; however, because the Z -function correction points are usually close to the exact MPP's, the AMV solution provides a reasonably good solution.

The AMV solution can be improved by using an improved expansion point, which can be done typically by an optimization procedure or an iteration procedure. Based initially on Z_{MV} and by keeping track of the MPPL, the exact MPP for a particular limit state $Z(X) - z_0$ can be computed to establish the AMV+ model, which is defined as

$$Z_{AMV+} = Z(x^*) + \sum_{i=1}^n \frac{\partial Z}{\partial X_i} \Big|_{x_i^*} (X_i - x_i^*) + H(X) \quad (6)$$

where x^* is the converged MPP. The AMV-based methods have been implemented in NESSUS and validated using numerous problems⁶.

Probabilistic Sensitivity Analysis

For design purposes, it is important to know which problem parameters are the most important and the degree to which they control the design. This can be accomplished by performing sensitivity analyses. In a deterministic analysis where each problem variable is single-valued, design sensitivities can be computed that quantify the change in the performance measure due to a change in the parameter value, i.e., $\partial Z/\partial X_i$. The sensitivity computed as a by-product of MPP-based methods is

$$\alpha_i = \frac{\partial \beta}{\partial u_i} \quad (7)$$

measures the change in the safety index with respect to the standard normal variate u .

Probabilistic Analysis

Probabilistic Response of Valve – Piston Assembly

Material stress-strain curves and impact loading parameters are treated as *random variables* with a given probability density function (PDF) having a specific distribution-type with a mean (μ) and standard deviation (σ). As noted earlier, the non-normal distributions are mapped into a normal distribution in u -space. A probabilistic structural response analysis is conducted showing the overall probability of failure (p_f) of the component to the input loads, for the

imposed limit state (or failure criteria). Also, quantitative and qualitative sensitivity factors are presented showing random variables that have (and those that do not have) a large effect on the overall failure probability of the component.

Random Variable Functions. Table 3 through Table 5 depict the random variables used in this analysis along with the respective distributions. Impact loading parameters such as initial velocity and reaction products back-pressure are normally distributed. Further analysis of lead-styphnate reaction is required to determine an accurate characterization of the burn-exponent and burn-constant parameters for better approximations of the loading distributions. Nevertheless, the distributions shown in Table 5 for the burn variables are considered acceptable.

Table 3. Piston RV's

Parameter	Mean	σ	Distribution
E_p (psi)	29.E6	6.67E5	Log-normal
S_{VP} (psi)	235775.	23477.5	Log-normal
E_{HP} (psi)	96375.	9637.5	Log-normal
M_p (g)	12.0	0.23	Normal
Geom	0.055	0.0022	Normal

Table 4. Valve RV's

Parameter	Mean	σ	Distribution
E_v (psi)	29.E6	6.67E5	Log-normal
S_{Vv} (psi)	45000.	4500.	Log-normal
E_{HV} (psi)	209840.	20984.	Log-normal

Table 5. Impact Parameter RV's

Parameter	Mean	σ	Distribution
V_1 (in/s)	-2750.	131.	Normal
P_{RP} (psi)	12000.	1200.	Normal

Piston and valve material properties were allowed to have a log-normal distribution, which is consistent with material manufacturing observations. Statistical data is not readily available for these material lots, and therefore the distributions are speculative at best. However, ongoing material characterization will provide an accurate variation in piston and valve properties in the near future. The piston cutter ring thickness variation is shown in Figure 17, with the distribution as presented in Table 3.

Three separate methods of analyses were conducted to determine the efficiency and accuracy of the reliability algorithms within NESSUS. These were, MV (Mean Value), AMV (Advanced Mean Value), and LHS (Latin Hypercube Sampling). The LHS method⁹ was included to show the accuracy of AMV, without performing a full Monte Carlo analysis to the $\pm 3\sigma$ levels. These methods are described elsewhere in this paper.

Probabilistic Model Results

Results of the probabilistic model are presented in this section, including a sensitivity analysis and probabilistic results showing exceeding the limiting plastic shear strain of 30%, or a potential failure domain.

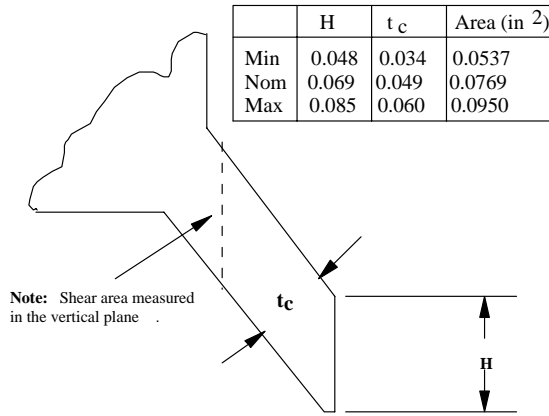


Figure 17. Piston ring thickness variability

Sensitivity Analysis. The information shown in Figure 18 represents the importance (i.e., sensitivity) of each random variable to the overall probability of exceeding the plastic shear strain, postulated to cause structural failure for the component.

The most important variables leading to prediction of structural failure are (1) flow characteristics of piston, (2) flow characteristic of valve, (3) impact velocity, and (4) cutter ring thickness. Of course, to a certain degree, the other random variables are important yet may, in and of themselves, not lead to structural failure. Each component's Young's Modulus, however, appears insignificant to the overall probabilistic response. As such, these two random variables could, in effect, have been maintained as deterministic variables without loss of generality in the results, and reduced the number of finite element analyses conducted under MV, AMV, and LHS.

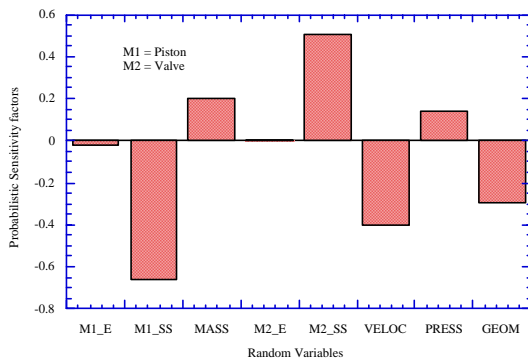


Figure 18. Importance factor for exceeding plastic shear strain.

Figure 19 and Figure 20 show cumulative distribution functions (CDF) depicting the (a) probability and (b) standard normal variate respectively, as a function of exceeding the plastic shear strain limit. The limit-state (or g -function) is merely the failure strain of the material minus the resulting

strain from the finite element model. Thus, the g -function is the following:

$$g(X) = Z(X) - z_0$$

where: $Z(X)$ = Limiting response function
and, z_0 = Response function

A g -function equal to zero represents the failure strain (or limit-state) of the material is equal to the resulting strain from the FEA model. These results imply a 50% probability of failure for the nominal conditions. In other words, there's a 50% probability of structural failure of the piston for the given nominal material state and loading parameters.

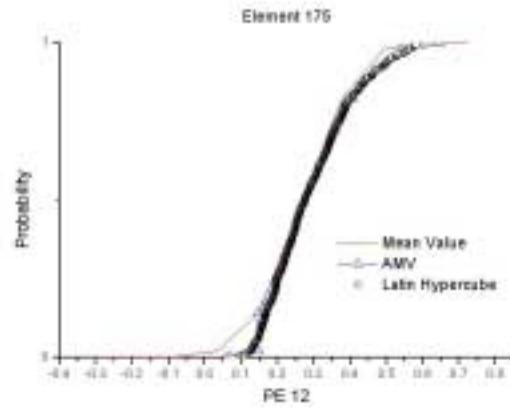


Figure 19. CDF for exceeding plastic shear strain.

Figure 20 shows similar information as Figure 19, but is based on the standard normal variate probability function. The ordinate plots the standard deviations from the mean, while the abscissa plots the actual total strain from the FEA model. Therefore, at the mean (μ), or at a standard deviation of zero ($\sigma = 0$) the exceeding plastic shear strain of 30% is reached.

The number of finite element model solutions necessary for the MV, AMV, and LHS is shown in Table 6. It is evident from Figure 20, and Table 6, that the AMV method is quite efficient as compared to the LHS. The MV results appear to deviate into physically inadmissible regions, such that it predicts absolute value shear strains which are negative. However, this result is corrected by the AMV method.

Table 6. FEA Solutions

Method	FEA Runs
MV	65
AMV	9
LHS	500

The AMV and LHS results follow closely throughout the CDF. Especially in regions away from the mean and nearing the $\pm 3\sigma$ levels, the AMV results are nearly identical to the LHS. The powerful and efficient methods employed in NESSUS make it extremely attractive in solving large models with the minimum number of numerical solutions.

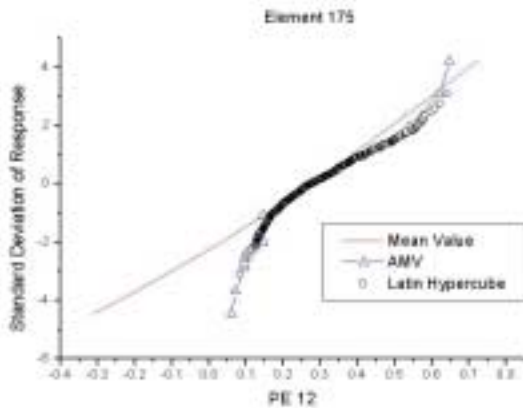


Figure 20. Standard normal CDF for exceeding plastic shear strain.

The analysis provided in this paper attempts to show, both in a deterministic and probabilistic methodology, that the original design for this piston/valve system is marginal, at best. Furthermore, performing a probabilistic analysis using the probabilistic code NESSUS coupled to ABAQUS/Explicit, provides a much more efficient means of achieving the reliability of a component to the given random variable distribution. The deterministic sensitivity analysis amounted to 12 finite element solutions without a clear knowledge of the failure domain. Conversely, efficient reliability methods in NESSUS provides a complete CDF solution with the minimum number of solutions. The attractive feature of using PSAM is that alternatives may be developed during design stages that enhance the reliability of a component or system. More importantly, the efficient reliability algorithms employed in NESSUS provide the accuracy without the expense of a full Monte Carlo analysis.

Probabilistic Response of Float

In order to capture, as simply as possible, the total structural response of a float under collapse, it was decided to perform a probabilistic analysis at the point of maximum force during buckling. The maximum force needed to crush the float occurs at a platen stroke of approximately 6 inches. For the first 4.5 inches, the top and bottom of the float dimple inward. The float is buckling for the next 1.5 inches leading up to the point of maximum force. After this point, the float will be compressed to such an extent that it begins to act like a solid piece of steel between the two platens.

To date, a comprehensive investigation of float geometry and material characteristics has not been accomplished. The outside contours of all the floats, however, have been measured and statistical data on the radius is available. Due to this lack of statistical data, the decision was made to perform a simple probabilistic analysis using four random variables and using judgement where appropriate.

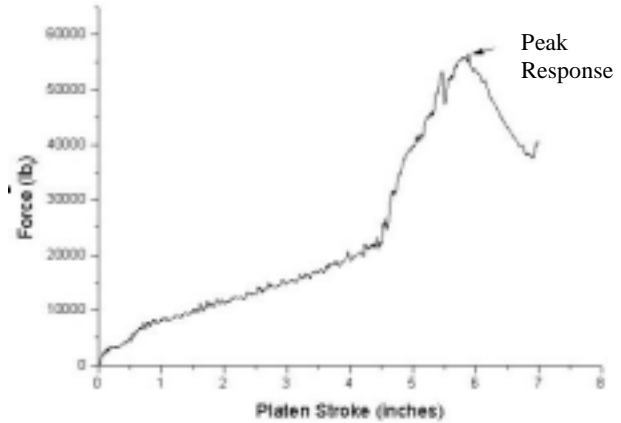


Figure 21. Response used in the probabilistic analysis.

The random variables are modulus of elasticity, yield stress, radius, and thickness of the steel plate. The coefficients of variation (COV) for modulus of elasticity and yield stress are taken from a handbook⁸ for 304 stainless steel. The COV for radius was calculated from the outside contour information. An assumption is made that the manufacturing tolerance for the thickness of the steel plates is equivalent to the tolerance for radius. Therefore, the COV's for thickness and radius are equal.

Table 7. Probabilistic Data for the random variables.

Random Variable	PDF	COV
E	Lognormal	0.0238
S _y	Normal	0.10
radius	Normal	0.00158
thickness	Normal	0.00158

The CDF of the response function, point of maximum force, was calculated using NESSUS and plotted in x- and u-space. Figure 22 and Figure 23 show the results from the Mean Value and Advanced Mean Value analyses. A limited Monte Carlo analysis using twenty sampling points has been included to validate the results.

The Mean Value method, a simple, linear approximation of the response about the mean, matches nicely with the twenty Monte Carlo points. The Advanced Mean Value method is a perturbation about the MV solution and is intended to improve the solution about the tails of the CDF. In this case, the upper tail of the AMV solution seems to diverge from the Monte Carlo samples. Although not thoroughly investigated at this point, it is currently believed that small perturbations in the random variables can occasionally alter the buckling characteristics of the float. A change in the buckling pattern can result in different structures that could weaken or strengthen the float. This phenomenon can cause the response function to be non-linear.

Work is currently underway to characterize the spatial variations in material properties and geometry in an effort to get closer agreement with experimental results.

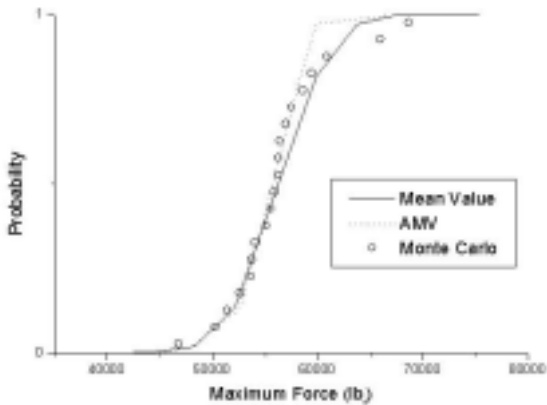


Figure 22. CDF of the response function.

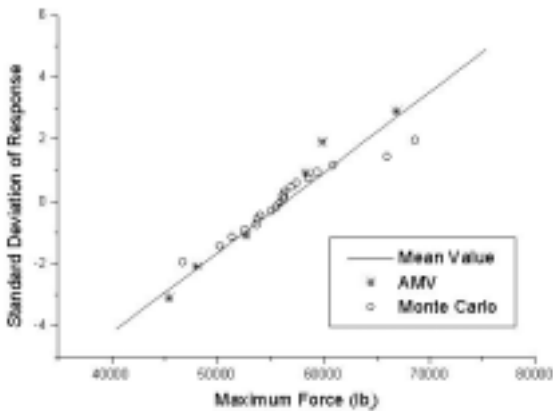


Figure 23. CDF of the response function in u-space.

The question remains on the appropriateness of using the maximum buckling load as the response function for this problem. Further investigation is needed to determine conclusively if perturbations in the dependent variables are causing a non-linear response in the buckling load. Additionally, a better understanding of the different buckling characteristics of the float is required. Also, it may be necessary to consider using a response function other than the maximum buckling force, such as the total work done in crushing.

Finally, once a proper interrogation of float geometry and material has been accomplished and statistical data is available, a more detailed and accurate probabilistic analysis will be completed. Currently, the thickness of the steel plates is taken to be constant throughout each hemisphere. If statistical data finds thickness to vary from equator to pole in terms of mean, standard deviation, and type of PDF, this information can be incorporated in the model.

A range of buckling loads has been determined and in Figure 24, the importance of the dependent variables on the maximum buckling load can be examined.

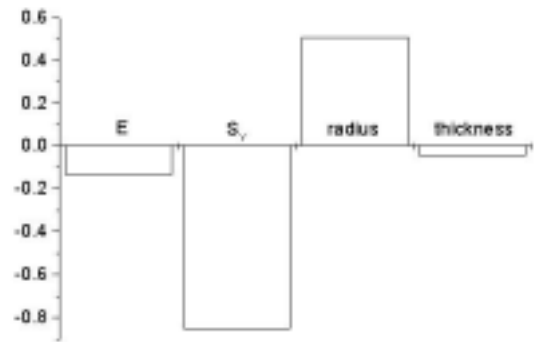


Figure 24. Sensitivity factors (α) of the random variables.

Conclusion

The probabilistic analysis documented here demonstrates the power and usefulness of NESSUS. Using the efficient algorithms of the Advanced Mean Value method can provide valuable insight above and beyond the deterministic analysis. The continued application of probabilistic analysis methods is needed to develop the needed tools and experience to support weapon certification.

Acknowledgement

Support from Los Alamos National Laboratory, which is operated by the University of California, under Contract No. W-7405-ENG-36 with the US Department of Energy (DOE) is gratefully acknowledged.

References

- Holt, J. M., technical editor, *US Air Force Structural Alloys Handbook*, Vol. 2, CINDAS/Purdue University, 1992.
- NESSUS User's Manual, Southwest Research Institute, SwRI, 1998.
- Hibbitt, Karlsson, and Sorensen, *ABAQUS/Explicit User's Manual*, HKS, Inc., Providence, RI, 1998.
- Wu, Y. T. and Burnside, O. H., *Efficient Probabilistic Structural Analysis Using an Advanced Mean Value Method*, Proceedings, ASCE Specialty Conference on Probabilistic Mechanics, 1988.
- Whirley, R. and Engelmann, B., *DYNA3D User Manual*, Lawrence Livermore National Laboratory report UCRL-MA-107254, Rev. 1, Dec. 1988.
- Thacker, B. H., et al., *Computational Methods for Structural Load and Resistance Modeling*, AIAA-91-0918-CP, April 1991.
- Wu, Y. T., et al., "Advanced Probabilistic Structural Analysis Method for Implicit Performance Functions," *AIAA Journal*, Vol. 2, No. 9, Sept. 1990.
- Haugen, E. B., *Probabilistic Mechanical Design*, Wiley, 1980.
- McKay, M. D., et al., "A Comparison of Three Methods for Selecting Values of Input Variables in the Analysis of Output from a Computer Code," *Journal of Technometrics*, Vol. 21, No. 2, May 1977.